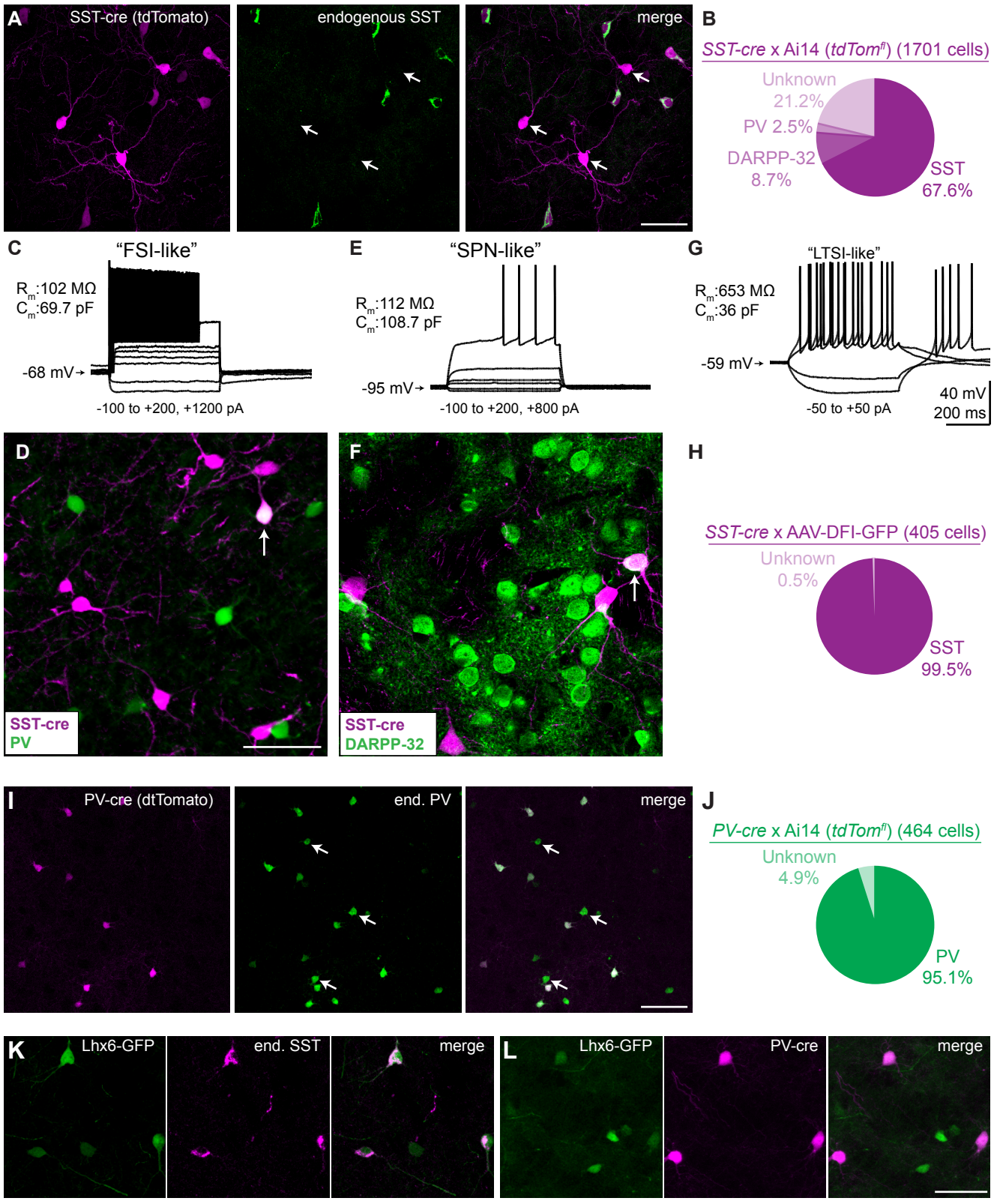

Figure S1
(refers to Figure 1)

Figure S1 (refers to Figure 1): Specificity and selectivity of transgenic mouse lines used to label LTSIs and FSIs.

(A) A subset of tdTomato-positive cells (magenta) in the striatum of SST-cre mice crossed to tdTomato reporter mice (Ai14) do not express endogenous SST (green) in the adult animal (arrows). Similar results have been described for the same mouse line in cortex (Pala and Petersen, 2015).

(B) Distribution of tdTomato-positive cells as described in (A). About one third do not express endogenous SST, and within this group small subsets express PV (FSI marker) or DARPP-32 (SPN marker). No overlap with ChAT (CIN marker) was found.

(C-F) In agreement with expression of PV (D, arrow) or DARPP-32 (F, arrow) some tdTomato-positive cells in the striatum of SST-cre mice crossed to tdTomato reporter mice showed electrical phenotypes typical for FSIs ((C) 2/24 cells; intermediate capacity and input resistance, paired with high maximal firing rates (Gittis et al., 2010)) or for SPNs ((E), 4/24 cells; negative resting potential, large capacity, delayed-onset spiking (Kreitzer, 2009)). These data indicate that cre expression throughout development is not limited to LTSIs, but also can also appear in FSIs or SPNs, respectively.

(G, H) When identified by viral expression of a cre-dependent marker (DFI-GFP) delivered at P18-22, cre expression is faithfully restricted to SST-positive cells in the striatum of SST-cre mice (H), and under these conditions all GFP-positive cells also show electrical phenotypes reminiscent of LTSIs ((G), high input resistance, small capacity, and rebound-spiking (Gittis et al., 2010)). Together, these results indicate a transient expression of cre in a subset of other cells during development in the striatum of SST-cre mice, but using viral delivery at a juvenile age can circumvent this unfaithful expression.

(I, J) Same as in (A, B), but for PV-cre mice. In this line, cre-expression throughout development in striatum was largely restricted to neurons that also expressed endogenous PV in adult animals. However, only 72.5% (182/251) of all PV-positive cells expressed cre (arrows indicate PV-positive, cre-negative cells).

(K) 94.3% of SST-positive cells (magenta) were also positive for GFP (green) in Lhx6-GFP mice (383/406 cells, arrows).

(L) 72.5% of all tdTomato-positive cells (87/120 cells, arrows) were also GFP-positive in PV-cre mice crossed with tdTomato reporter and Lhx6-GFP mice. Scale bars: 50 μm and 200 μm (I).

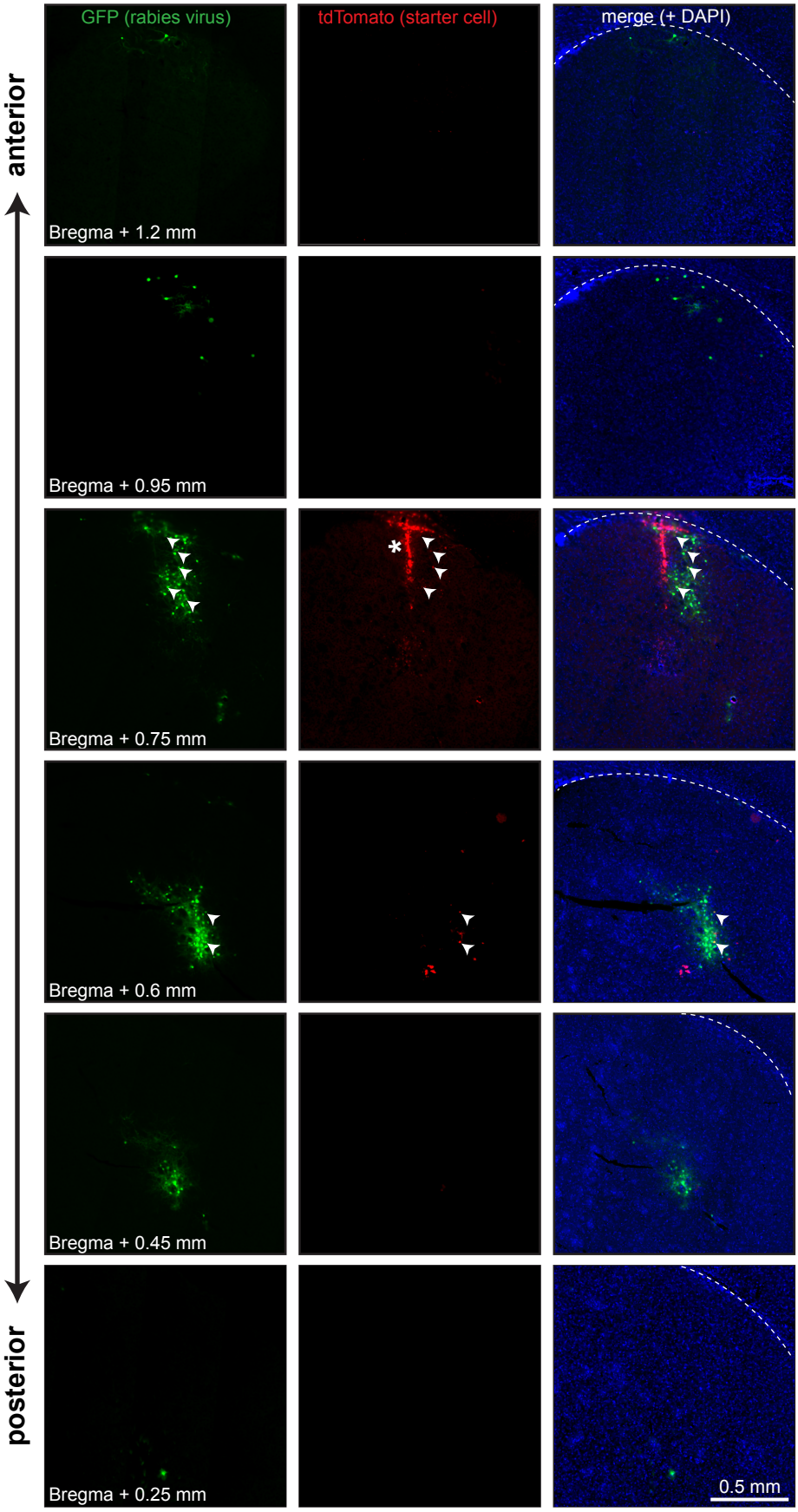

Figure S2
(refers to Figure 3)

Figure S2 (refers to Figure 3): Representative example of rabies tracing experiment in dorsal striatum.
Coronal striatal sections from different anterior-posterior positions, relative to Bregma, surrounding the injection site (Bregma 0.75 mm; asterisk indicates injection tract). Rabies virus is in green *(left),* starter virus expression in red *(middle)*, and DAPI in blue *(right)*. Note that rabies virus-expressing cells spread over a larger volume than starter cells, reflecting monosynaptically connected cells. Arrowheads indicate identified starter cells (i.e. green/ red double-positive cells), and can be found in this example at the injection site and up to 0.15 mm posterior (Bregma +0.6 mm). Dashed white line indicates callosal-striatal border.

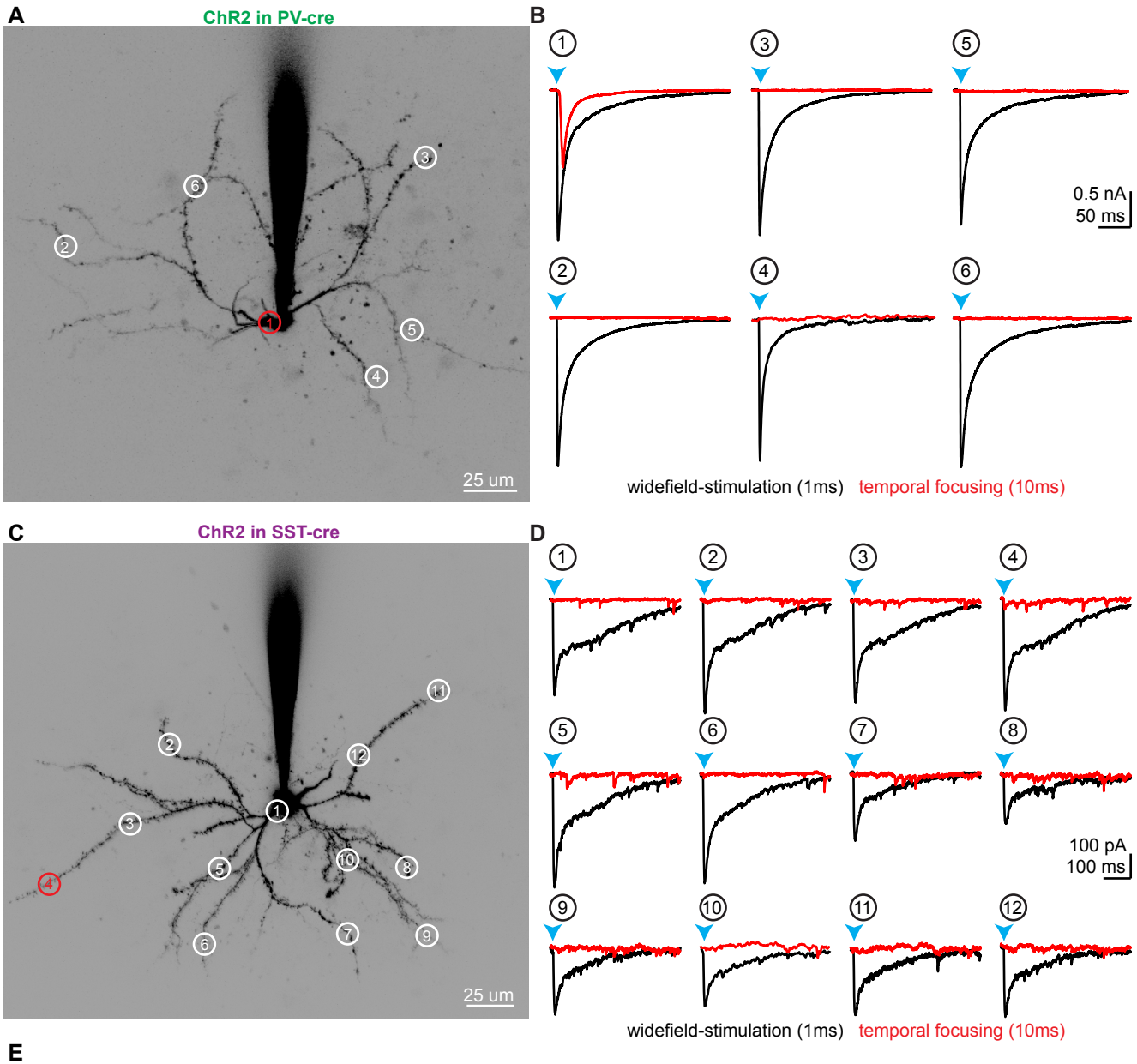

Figure S3
(refers to Figure 4)

Figure S3 (refers to Figure 4): Direct dendritic mapping of synapse location in SPNs, using temporal focusing subcellular ChR2-assisted circuit mapping.

(A, C) 2-photon (2P) images of recorded SPNs in PV-cre (A) or SST-cre (C) mice filled with AlexFluor594. Circled numbers indicate locations tested by TF 2P ChR2 activation, and red numbers indicate locations where synaptic currents were evoked.

(B, D) Currents evoked for TF 2P ChR2 activation locations indicated in (A, C). For each location, widefiled-stimulation (black traces) and TF activation (red traces) were interleaved, and cells were only used when widefield stimulation evoked reliable currents. In PV-cre mice synaptic currents could always be evoked by TF activation at the cell body (7 cells from 3 mice), but never at dendritic sites (19 locations on 7 cells). In contrast, in SST-cre mice TF activation did never evoked synaptic currents at the cell body (13 cells from 4 mice), but in 131 locations on 13 cells one dendritic synaptic site could be identified (number 4 in C, D). Note that the experiments were performed in TTX/4-AP, and decay kinetics of synaptic currents are slower due to inhibited re-polarization of presynaptic terminals.

(E) Magnification of TF 2P ChR2 evoked currents for locations 1, 4, and 11 from (C, D). Only position 4 showed reliable currents, i.e. currents of at least unitary size that could be evoked in every sweep (gray traces). Red traces shows averages.

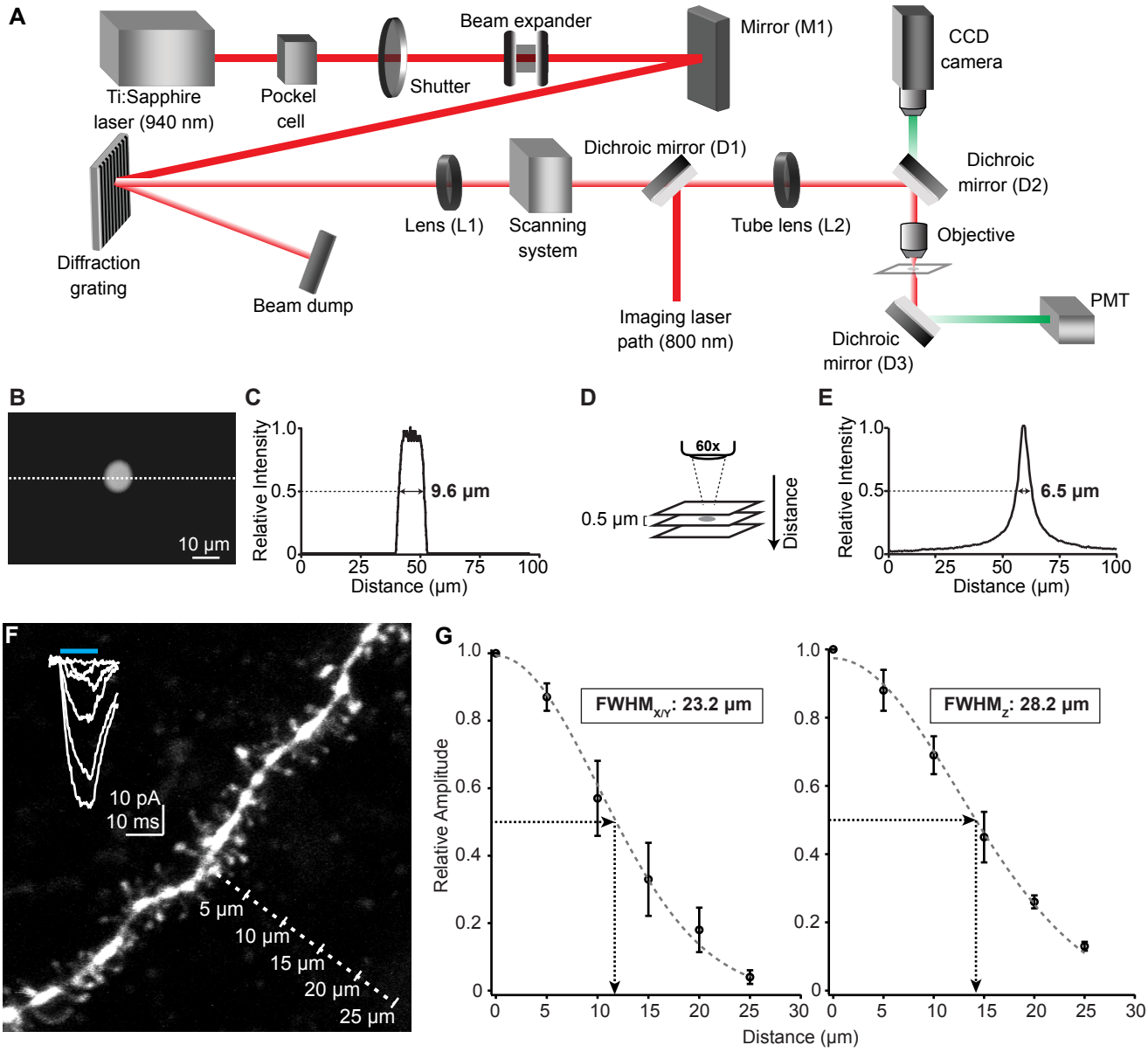

Figure S4
(refers to Figure S3 and Figure 4)

Figure S4 (refers to Figure S3 and Figure 4): Characterization of temporally focused 2-photon ChR2 activation.

(A) Schematic layout of the microscope used for temporal focusing. Technical details of the temporal focusing pathway, including part numbers and specifications, are described in the supplemental methods. The temporal focusing pathway was combined with a 2-photon (2P) imaging system as described before (Carter and Sabatini, 2004), to yield a microscope that could be used for simultaneous 2P imaging and temporally focused 2P activation of ChR2.

(B) To measure the X/Y dimension of the resulting laser spot, the temporal focusing spot was flashed on a layer of fluorescein between a microscope slide and a coverslip, and epifluorescence was detected on the CCD camera (top).

(C) Fluorescence intensity profile along the dotted line shows a full-width half-maximum (FWHM) of 9.6 μm (bottom).

(D) The axial resolution of the TF system was measured by illuminating a thin layer of Rhodamin6G (a gift from Valentina Emiliani, Paris) with the temporal focusing spot, and integrating the fluorescence of the spot on the bottom PMT. A stack of the fluorescence was acquired every 500 nm as the spot's focus was displaced by moving the objective from 50 μm above to 50 μm below the coverslip (top).

(E) The resulting intensity profile (bottom) shows a FWHM of 6.5 μm.

(F) To measure the actual resolution of dendritic ChR2 activation in scattering tissue the laser spot was placed directly onto a dendrite of a ChR2-expressing SPN filled with Alexa Fluor594, and then moved away in 5 μm increments. The resulting currents of the example shown here are displayed on the top left.

(G) Normalized current amplitudes were fit to a Gaussian distribution, and yielded a FWHM of 23.2 μm in X/Y-direction and 28.2 μm in Z-direction (n = 6 cells).

Table S1 (refers to Figure S4): Temporal focusing microscope part specifications.

Part	Reference
Ti:Sapphire laser	Coherent Chameleon Vision II
Pockel Cell	350/302M, Conoptics
Shutter	LS6Z2 Uniblitz, Vincent Associates
Beam expander	AC254-200-B-ML and AC508-150-B, Thorlabs
Mirror M1	BB1-E03, BB2-E03, Thorlabs
Diffraction grating	53107BK01-520R, Newport
Lens L1	AC508-100-B-ML, Thorlabs
Scanning System: Galvanometric mirrors Relay lenses	 5mm fan shape, 6215 HB Cambridge technology FV-PL-W3, Olympus
Dichroic Mirror D1	custom made from filter ff01-945/sp-25, Semrock
Tube Lens L2	LA1979-B, Thorlabs
Dichroic Mirror D2	700DCXR, Chroma technologies
Objective	LUMPlanFl/IR 60x 0.9 NA, Olympus
Dichroic Mirror D3	FF705-Di01-52x63, Semrock
Photomultiplier Tube	R3896, Hamamatsu
CCD Camera	Teli CS8320B, Toshiba

SUPPLEMENTAL EXPERIMENTAL PROCEDURES

Mice: IRES-cre-knockin mice expressing cre-recombinase under the control of *somatostatin* (stock number 013044 (Taniguchi et al., 2011); RRID:IMSR_JAX:013044) or *parvalbumin* (stock number 008069 (Hippenmeyer et al., 2005); RRID:IMSR_JAX:008069) were obtained from the Jackson Laboratory, and are referred to here as Somatostatin-cre (SST-cre) and Parvalbumin-cre (PV-cre) mice, respectively. BAC-transgenic mice expressing cre (*Adora2a*-cre, founder line KG139; RRID:MMRRC_031168-UCD) or eGFP (*Drdr2*-eGFP, founder line S118; RRID:MGI:4830460) in striatal projection neurons (SPNs) of the indirect pathway, or cre in SPNs of the direct pathway (*Drd1a*-cre, founder line EY262; RRID:MGI:5660866) were developed by the Gensat project (Gong et al., 2003). BAC-transgenic mice expressing eGFP in GABAergic interneurons (Gittis et al., 2010) (*Lhx6-GFP* mice, Gensat, founder line BP221; RRID:MMRRC_000246-MU) were kindly provided by Dr. M. Levine (UCLA). To visualize cre-expression, mice were crossed to Ai14 reporter mice (Jackson Laboratory, stock number 007914 (Madisen et al., 2010); RRID:IMSR_JAX:007914), which carry a floxed tdTomato reporter transgene. All animals were maintained on a C57Bl/6 background. Unless generating double-transgenic mice, one transgenic breeder (of either sex) was crossed to a wildtype mouse, and all experiments were performed using heterozygous offspring. Experimental manipulations were performed in accordance with protocols approved by the Harvard Standing Committee on Animal Care following guidelines described in the US National Institutes of Health *Guide for the Care and Use of Laboratory Animals*.

Surgery: Stereotaxic intracranial injections were used to virally deliver ChR2 for electrophysiological recordings in SST-cre, PV-cre, or A2A-cre mice, or rabies virus for tracing of synaptic inputs in D1-cre mice. Mice (P18 - 22) were anesthetized with isoflurane, placed in a stereotaxic frame (David Kopf Instruments), and the skull was exposed under aseptic conditions. For electrophysiological recordings in dorsal striatum (see below for details on rabies injections) a small hole was drilled into the skull unilaterally and 1 µl of an adeno-associated virus (AAV, serotype 2/8) encoding double-floxed inverted ChR2(H134R)-mCherry ($\geq 10^{12}$ genomic copies per milliliter, UNC Vector Core) was injected through a pulled glass pipette at a rate of 100 nl/min using a UMP3 microsyringe pump (World Precision Instruments). Following injection, the pipette was left in place for ~15min, in order to avoid back spill of the virus. Injection coordinates were 0.75 mm anterior of Bregma, 1.9 mm lateral, and 2.45 mm below pia. After surgical procedures, mice were returned to their home cage for 18 - 22 days to allow for sufficient expression.

Slice Preparation: Acute brain slices were obtained from mice at P40 - P45 using standard techniques (Straub et al., 2014). Mice were anaesthetized by isoflurane inhalation and perfused transcardially with ice-cold artificial cerebrospinal fluid (ACSF) containing (in mM) 125 NaCl, 2.5 KCl, 25 $NaHCO_3$, 2 $CaCl_2$, 1 $MgCl_2$, 1.25 NaH_2PO_4 and 11 glucose (295 mOsm/kg). Cerebral hemispheres were removed, placed in cold choline-based cutting solution (consisting of (in mM): 110 choline chloride, 25 $NaHCO_3$, 2.5 KCl, 7 $MgCl_2$, 0.5 $CaCl_2$, 1.25 NaH_2PO_4, 25 glucose, 11.6 ascorbic acid, and 3.1 pyruvic acid), blocked and transferred into a slicing chamber containing ice-cold choline-based cutting solution. Parasagittal slices of striatum (275 µm thick) were cut with a Leica VT1000 s vibratome, transferred for 10–20 min to a holding chamber containing ACSF at 34 °C and subsequently maintained at room temperature (20–22 °C) until use. All recordings were obtained within 4 h of slicing. Both cutting solution and ACSF were constantly bubbled with 95% O_2/5% CO_2.

Electrophysiology: Individual slices were transferred to a recording chamber mounted on an upright microscope (Olympus BX51WI) and continuously superfused (2–3 ml/min) with ACSF warmed to 33–34 °C by passing it through a feedback-controlled in-line heater (SH-27B; Warner Instruments). Cells were visualized through a 40x or 60x water-immersion objective with either infrared differential interference contrast (DIC) optics or epifluorescence to identify ChR2–$mCherry^+$ interneurons or SPNs. Whole-cell voltage- and current-clamp recordings were made from cells in anterior dorsolateral and dorsomedial striatum within 400 µm of the callosal-striatal border. SPNs and cholinergic interneurons (CINs) were identified based on their morphology and electrical properties, and GABAergic interneurons were identified by mCherry expression in SST+ or PV+ cells, respectively. Patch pipettes (2.2 - 3.5 MΩ) pulled from borosilicate glass (G150F-3, Warner Instruments) were filled either with a Cs^+-based high Cl^- internal solution containing (in mM) 125 CsCl, 10 TEA-Cl, 10 HEPES, 0.1 EGTA, 3.3 QX-314 (Cl^- salt), 1.8 $MgCl_2$, 4 Na_2-ATP, 0.3 Na-GTP, 8 Na_2-phosphocreatine (pH 7.3 adjusted with CsOH; 295 mOsm/kg) for voltage-clamp recordings, or with a K^+-based low Cl^- internal solution composed of (in mM) 130 $KMeSO_3$, 5 KCl, 10 HEPES, 0.2 EGTA, 1.8 $MgCl_2$, 0.1 $CaCl_2$, 4 Na_2-ATP, 0.3 Na-GTP (pH 7.3 adjusted with KOH; 295 mOsm/kg) for current-clamp recordings. For recordings using temporally focused 2-photon activation of ChR2 or glutamate

uncaging, Alexa Fluor594 (10 μM, Invitrogen) was added to the internal solution. Extracellular solutions for current-clamp recordings did not contain drugs unless specified otherwise, but for voltage-clamp recordings AMPA- and NMDA-type glutamate receptor antagonists NBQX and CPP (10 uM each) were included in all recordings, except for glutamate uncaging (see below). Under these conditions $GABA_A$ receptor mediated chloride currents were isolated as inward currents at negative holding potentials (V_{hold} = -70 mV, unless otherwise noted). For all voltage-clamp experiments, errors due to the voltage drop across the series resistance (<20 MΩ) were left uncompensated. Since a high-chloride pipette solution was used, liquid junction potential was not corrected for. To activate ChR2-expressing fibers, light from a 473 nm laser (Optoengine) was focused on the back aperture of the microscope objective to produce wide-field illumination of the recorded cell. Brief pulses of light (1 ms duration; ~3 mW/mm^2 on the sample, unless otherwise noted) were delivered through the objective at 15 s intervals under control of the acquisition software. Drugs were bath applied at the indicated concentrations.
For voltage-jump experiments, cells were clamped alternately at -40 mV constantly or at 0 mV first (the reversal potential for chloride under the present recording conditions), followed by a step to -40 mV. The step to -40 mV occurred either 20 ms after optogenetic activation of the respective GABAergic input, 10 ms into a 12 ms-light pulse when using temporally focused 2-photon activation of ChR2 in SPNs, or 8ms after the first uncaging pulse when using glutamate uncaging. The currents evoked by just applying the voltage step without optogenetic activation were monitored in interleaved trials and subsequently subtracted from the trials with optogenetic stimulation. This approach cancels both passive (including capacitive) and active currents generated by the voltage step and isolates the synaptic component of ChR2-mediated currents.
For glutamate uncaging MNI-caged-L-glutamate (3 mM, Tocris) was added to the bath solution and activated by a 2 ms light pulse of a Ti:Sapphire laser tuned to 720 nm, directed next to a morphologically identified spine-head (visualized by imaging AlexaFluor594-containing cell fill with a second Ti-Sapphire laser, tuned to 820 nm). In order to maximize current amplitudes for voltage jumps experiments in distal dendrites, synapses on three neighboring spines were activated consecutively (333 Hz) at high power-levels (8 to 34 mW, depending on the depth of the uncaging site). To further increase current amplitude, cyclothiazide (100 μM) was added to the bath solution, and baseline activation by ambient glutamate levels was prevented by adding TTX (1 μM), CPP (10 μM), and the glutamate scavenger glutamine-pyruvate-transferase (GPT; 5 units/ml) with sodium-pyruvate (2 mM).
Two alternative approaches were used to determine minimal synaptic events. Quantal events were measured by desynchronizing presynaptic release with strontium. In these experiments ACSF was replaced by a strontium-containing, calcium-buffered bathing solution as described before (Xu-Friedman and Regehr, 1999), containing (in mM): 120 NaCl, 34 $NaHCO_3$, 2.5 KCl, 1 $MgCl_2$, 1.25 NaH_2PO_4, 2 EGTA, and 4 $SrCl_2$ (295 mOsm/kg). Synaptic events were identified and analyzed using standard software for detection of mEPSCs in a window from 50 to 150 ms post-stimulus. Alternatively, a minimal stimulation protocol was used to record unitary currents: laser power was reduced (0.2 - 0.6 mW/mm^2) while simultaneously moving away from the recorded cell (175 - 915 μm), until failures appeared. To determine decay kinetics of unitary events, 20 – 30 individual strontium-evoked events with clear rise and decay phases were selected for each cell, aligned at 50% rise time, and averaged, to represent one data point.

Temporal Focusing: A custom-built microscope was used for temporally focused 2-photon activation of ChR2, utilizing a Ti:Sapphire laser tuned to 940 nm. The laser output was controlled by a Pockel cell and expanded to obtain the desired beam size on a diffraction grating. Diffracted light was collected by a lens before entering the scanning module composed of two galvanometric mirrors coupled by a telecentric relay. Finally, the beam was coupled to the tube lens of the microscope with a third scanning lens and a dichroic. In this way, the plane of the diffraction grating was relayed to the focal plane of the objective (i.e. the specimen plane), where the mirrors were conjugated with the back focal plane of the objective to allow for scanning the larger spot in the field. The magnification chosen here translated into a spot of 9.6 μm in diameter and an axial confinement of 6.5 μm (FWHM). For recordings, cells were filled with Alexa Fluor594, and visualized using a second Coherent Ultra II laser (800 nm). The temporally focused laser spot was placed onto the desired location along the dendritic tree. To further reduce the chance of contamination by ChR2-activation in other dendrites, experiments were performed on dendrites that were clearly isolated both in X/Y and Z. The actual resulting resolution of ChR2 activation in scattering tissue is lower than the theoretical beam size, and characterized in Suppl. Fig. 4. The pathway of the temporal focusing module is schematized in Suppl. Fig. 4, and individual optical components are specified in Supplemental Table 1. Laser power was ~60 to 100 mW under the objective throughout all experiments.

Data Acquisition and Analysis: Membrane currents and potentials were amplified and low-pass filtered at 3 kHz using a Multiclamp 700B amplifier (Molecular Devices), digitized at 10 kHz (or 100 kHz for voltage jumps) and

acquired using National Instruments acquisition boards and a custom version of ScanImage written in MATLAB (Mathworks) (https://github.com/bernardosabatinilab/SabalabSoftware_Nov2009.git). Data were analyzed offline using Igor Pro (Wavemetrics), and average waveforms of 3-10 consecutive acquisitions were used for analysis and display, unless otherwise noted. Baseline was calculated as the average 100 ms before light pulse. Peak amplitudes were calculated by averaging over a 1ms window around the peak, and decay or rise constants were calculated by fitting the appropriate phase to an exponential. In some cases, currents were better described by double-exponential fits, and in these cases the weighted tau-values were calculated for statistical comparison.
For analyzing quantal events using strontium, spontaneous activity in a window from 50-150 ms post-pulse was analyzed using a custom-written script. Only experiments in which strontium at least doubled spontaneous activity in this time window were used for analysis, to ensure that the majority of events originate from the activated presynaptic cell type. For minimal-stimulation experiments, the maximal inward deflection from baseline 5-20 ms post-stimulus was used as amplitude, and for each trace the same analysis 10 ms pre- to 5 ms post-stimulus was used to define noise levels. Histograms were calculated using 5 ms bins, and binned data were fit with a Gaussian distribution as described in the text.
Data are represented as mean $\pm$ S.E.M. (bars), superimposed on individual data points (circles). Numbers of experiments are given as number of cells/ animals. Statistical analysis was performed in Prism (Graphpad Software), and data were compared using the nonparametric Mann–Whitney test (for group comparisons) or the nonparametric Kruskall–Wallis ANOVA followed by Dunn's test (for multiple group comparisons), unless noted otherwise. P-values smaller than 0.05 were considered to indicate statistical significant difference between groups.

Immunohistochemistry: Deeply anesthetized mice were perfused transcardially with 4% paraformaldehyde in 0.1 M phosphate buffer (pH 7.3) and brains were postfixed for 4 h at 4°C. 40 µm sections were cut on a vibratome (Leica) and processed free-floating. After blocking in 6% normal goat serum (NGS; or normal horse serum for primary antibodies raised in goat) with 0.2% Triton X-100 in phosphate buffered saline for 1 h at room temperature (or in Tris-buffered saline, containing 0.2% Tween-20 for DARPP-32 staining), sections were incubated in primary antibody overnight, followed by 1–2 h at room temperature in secondary antibody (in 3% NGS). Sections were mounted in ProLong Antifade Diamond reagent with DAPI (Invitrogen), and imaged with a slide-scanning microscope (VS120, Olympus). High-resolution images of regions of interest were subsequently acquired with a Leica LS8 confocal microscope (Harvard NeuroDiscovery Center). Individual imaging planes were overlaid and quantified for co-localization in NIH ImageJ. Confocal images represent maximum intensity projections of 15 µm confocal stacks.

Trans-synaptic Viral Tracing: For tracing studies using rabies virus, D1-cre mice (P20 - 24) were injected bilaterally with a lentivirus encoding for TVA receptor, B19G rabies glycoprotein and tdTomato in a cre-dependent manner with 2A cleavage sites between each protein (LV-EF1a-DIO-TVA-RVG-tdTom, $\geq 10^{11}$ infectious units/ml, 100 nl per hemisphere, at 50 nl/min; virus production: BCH Viral Core). Injections were as described above with coordinates 0.75 mm anterior of Bregma, 1.8 mm lateral, 2.7 mm below pia. Following expression for three weeks, mice underwent a second surgery, and a pseudotyped rabies virus encoding for eGFP (EnvA-SADΔG-EGFP, $\sim 10^9$ infectious units/ml, 200 nl, at 50 nl/min) was injected into the same location. The recombinant rabies viruses were generated in-house using BHK-B19G and BHK-EnvA cells, based on protocols similar to those previously described (Wickersham et al., 2010). Viral constructs for both the lentivirus and the rabies virus were kindly provided by Byung Kook Lim (UCSD). 7 days after rabies virus injection mice were processed for immunohistochemistry as described above, and coronal sections covering the entire striatum were mounted sequentially. For each mouse one hemisphere was processed for PV-staining and the other hemisphere for SST-staining, and the secondary antibodies were Alexa Fluor 647 coupled. Following image acquisition of an entire data set with a slide scanner microscope (VS120, Olympus), a set of custom-written macros in NIH ImageJ (Dr. L. Ding, Harvard NeuroDiscovery Center) were used to reconstruct each hemisphere into a three-dimensional volume, detect cells based on type (tdTomato/red: possible starter cell; eGFP/green: rabies virus expressing cell; Alexa647/ far red: PV or SST-interneuron), determine the x/y/z position of each starter cell (red/green double-positive) and monosynaptically connected interneuron of the respective type (green/far red double-positive), and calculate the linear distance between each connected interneuron and its closest starter cell. To quantify the spread of the starter cell population, starter cells across experiments were aligned by the center of mass, the distribution along each axis was fit with a Gaussian distribution, and the full-width half-maximum (FWHM) was measured.

Reagents: With the exception of GPT and sodium-pyruvate (Sigma), all drugs were from Tocris, and drugs were bath applied at the following concentrations: SR95531 (10 µM), 2,3-dihydroxy-6-nitro-7-sulfamoyl-

benzo(*f*)quinoxaline (NBQX; 10 µM), *R*,*S*-3-(2-carboxypiperazin-4-yl)propyl-1-phosphonic acid (CPP; 10 µM), tetrodotoxin (TTX; 1 µM), 4-aminopyridine (4AP; 200 µM), MNI-cgaed-L-glutamate (2 mM), cyclothiazide (100 µm), GPT (5 units/ml), sodium-pyruvate (2 mM). For immunohistochemistry, the following primary antibodies were used: rat anti-somatostatin (Millipore Cat# MAB354 RRID:AB_2255365, 1:500 dilution); rabbit anti-parvalbumin (Millipore Cat# MAB1572 RRID:AB_11211313, 1:2000); rabbit anti-DARPP-32 (Novus Cat# NB110-56929 RRID:AB_843832, 1:200); goat anti-ChAT (Millipore Cat# AB144P RRID:AB_11214092, 1:100). Respective secondary antibodies were from Invitrogen and coupled to Alexa Fluor 647, and used at a 1:500 dilution.

SUPPLEMENTAL REFERENCES

Carter, A.G., and Sabatini, B.L. (2004). State-dependent calcium signaling in dendritic spines of striatal medium spiny neurons. Neuron *44*, 483-493.

Gong, S., Zheng, C., Doughty, M.L., Losos, K., Didkovsky, N., Schambra, U.B., Nowak, N.J., Joyner, A., Leblanc, G., Hatten, M.E.*, et al.* (2003). A gene expression atlas of the central nervous system based on bacterial artificial chromosomes. Nature *425*, 917-925.

Hippenmeyer, S., Vrieseling, E., Sigrist, M., Portmann, T., Laengle, C., Ladle, D.R., and Arber, S. (2005). A developmental switch in the response of DRG neurons to ETS transcription factor signaling. PLoS Biol *3*, e159.

Kreitzer, A.C. (2009). Physiology and pharmacology of striatal neurons. Annu Rev Neurosci *32*, 127-147.

Madisen, L., Zwingman, T.A., Sunkin, S.M., Oh, S.W., Zariwala, H.A., Gu, H., Ng, L.L., Palmiter, R.D., Hawrylycz, M.J., Jones, A.R.*, et al.* (2010). A robust and high-throughput Cre reporting and characterization system for the whole mouse brain. Nat Neurosci *13*, 133-140.

Pala, A., and Petersen, C.C. (2015). In vivo measurement of cell-type-specific synaptic connectivity and synaptic transmission in layer 2/3 mouse barrel cortex. Neuron *85*, 68-75.

Taniguchi, H., He, M., Wu, P., Kim, S., Paik, R., Sugino, K., Kvitsiani, D., Fu, Y., Lu, J., Lin, Y.*, et al.* (2011). A resource of Cre driver lines for genetic targeting of GABAergic neurons in cerebral cortex. Neuron *71*, 995-1013.

Wickersham, I.R., Sullivan, H.A., and Seung, H.S. (2010). Production of glycoprotein-deleted rabies viruses for monosynaptic tracing and high-level gene expression in neurons. Nat Protoc *5*, 595-606.